RSC Advances

ROYAL SOCIETY OF CHEMISTRY

www.rsc.org/advances

Synthesis of micro/mesoporous silica material by dual-template method as a heterogeneous catalyst support for alkylation

Shuo Zhao, Man He, Yuming Zhou,* Xiaoli Sheng,*

Xiaoqin Fu, Yiwei Zhang

School of Chemistry and Chemical Engineering, Southeast University, Jiangsu Optoelectronic Functional Materials and Engineering Laboratory, Nanjing 211189, P. R. China. E-mail: ymzhou@seu.edu.cn (Y.Zhou); Tel: +86 25 52090617; Fax: +86 25 52090617.

Abstract

A series of micro/mesoporous composites were synthesized using non-ionic block copolymer Pluronic P123 and protic ionic liquid (triethylamine acetate) as the co-templates. The structures of all the composites were characterized by using small angle X-ray scattering, N_2 gas sorption, dynamic laser light scattering (DLS), scanning electron microscope (SEM) and transmission electron microscopy (TEM). The result reflected that the structure of the final silica materials change along with the content of protic ionic liquid (PIL) and hydrothermal temperature. It was found that the sample whose mass ratio of PIL to (P123+PIL) was 40% had a t-plot micropore area of 404 $m^2 \cdot g^{-1}$ at the hydrothermal temperature of 373 K, without destroying the ordered mesoporous structure. The formation mechanism of the micro/mesoporous silica which is based on the interaction between PIL and P123 is tentatively elucidated. 12-Tungstophosphoric acid (HPW) catalysts supported on these micro/mesoporous materials were prepared by impregnation, and their catalytic performances were investigated in the alkylation of *o-xylene* with styrene. Alkylation results showed that all the catalysts showed the high catalytic performance in terms of propane conversion and selectivity to propene.

1. Introduction

Since mesoporous silica materials were discovered,[1] hierarchical porous silica materials have received significant attentions due to their important role in the

systematic study of structure property relationship and their technological promise in applications.[2, 3] On one hand, hierarchical porous silica materials possess high surface area, large pore volumes and various frameworks like mesoporous materials, on the other hand, these materials have high thermal, hydrothermal and mechanical stability like microporous materials.[4-7] During the past decades, significant efforts have been devoted to design micro/mesoporous materials by using different approaches,[8, 9] such as postsynthetic demetalation process and template synthesis. And the approach using templates has been regarded as one of the most promising ways to obtain such this type of hierarchical porous silica materials.[10] These templates include the solid templates which contain carbon nanoparticles, ion-exchange resins and the soft materials which contain surfactants and colloids.[8, 9] The interaction between templates and siliceous precursors is very important to obtain the expected structures. Thus, it is crucial to find a series of appropriate templates.

Nowadays, ionic liquids (ILs), which are molten salts at room temperature, have attracted much interest due to their unique properties such as low vapor pressure, mild reaction condition, solvating ability, easy recycle ability and so on.[5, 11, 12, 13] Hence, the ionic liquids were actively studied by many research groups working in all kinds of fields, such as chemistry, organometallic, biocatalyzed reactions.[14, 15] ILs can act as multiple roles of cosolvent, cosurfactant as well as salt in the system.[16] So, ILs may greatly affect the aggregation behavior of aqueous surfactant solution. Long-chain amphiphilic ILs can self-assemble into ordered structures like surfactants.[17] Hence, ILs can induce micro or mesoporous materials.[18-20]

In the previous work, these inorganic materials were mostly prepared by imidazolium based ILs. Hu *et al.*[21] synthesized a high-quality cubic gyroid mesoporous silica (MCM-41) with the ionic liquid 1-hexadecyl-3-methylimidazolium bromide as the template under basic condition. Gao *et al.*[22] obtained a series of micro/mesoporous silica composites with P123 and imidazolium ILs ($[C_n mim]X$) as the cotemplates. They found that the structure of the materials changed along with the change of the alkyl chain length and anion. Hu *et al.*[23] synthesized the micro/mesoporous silicate materials using CTAB and imidazolium ILs ($[C_n mim]X$). They found the cations $[C_4 mim]^+$ can embed into CTA^+ micelles and aggregated into mixed micelles which acted as co-templates for synthesis of mesoporous materials at the room temperature, while at 373 K, the mixed micelles divided into CTA^+ micelles and $[C_4 mim]^+$ aggregates which were acted as mesoporous templates and microporous templates, respectively. So, imidazolium based ILs are appropriate to synthesize the micro/mesoporous silica materials.

The synthesis of highly ordered mesoporous silicate materials by a hydrothermal method has rarely been reported using protic ionic liquids (PILs) which are formed via the proton transfer from a Bronsted acid to a Bronsted base. Many PILs are miscible with water to form mixtures at any composition, and both the component ions favorably form hydrogen bonds with water.[24-26] Chen *et al.*[27] reported that the hierarchically nanostructured silica materials were obtained by using protic ionic liquid (ethylammonium nitrate) and non-ionic block copolymer pluronic P123 as templates through the sol-gel method. These materials contained a disordered

population of micropores and an ordered population of mesopores. And the micropores caused by ethylammonium nitrate. The micro/mesoporous materials, combining the advantages of mesoporous materials and microporous materials, are expected to be more suitable for catalytic reactions as catalysts support material. It is said that the product of Friedel-Crafts alkylation of *o-xylene* and styrene, 1-phenyl-1-xylyl ethane (PXE) is an appropriate solvent for many materials. In general, 12-Tungstophosphoric acid (HPW) and ordered mesoporous SBA-15 are used as acid catalysts and support, respectively to obtain PXE.[28, 29] Sheng *et al*.[30] successfully loaded HPW onto sulfonate-functionalized ionic liquid-modified mesoporous silica SBA-15 by total anion-exchange. And the final catalyst showed a high efficiency in alkylation. Thus, the micro/mesoporous materials can instead of the traditional supports to synthesize PXE to investigate if micro/mesoporous materials are suitable for this reaction.

In this work, a new approach to prepare miro/mesoporous silica materials possessing both micropores and mesopores has been suggested. The porous silica materials were synthesized with P123 and PIL (triethylamine acetate) as the co-templates by the hydrothermal method. A number of samples were synthesised by changing the PIL to P123 weight ratio and temperature during synthesis. Moreover, HPW supported on micro/mesoporous materials were prepared by impregnation method. The catalytic properties of the catalysts were assessed in the alkylation of *o-xylene* with styrene.

2. Experimental section

2.1 Chemicals

P123 ($PEO_{20}PPO_{70}PEO_{20}$) was purchased from Sigma-Aldrich, The inorganic silica precursor was silicon (IV) tetraacetate (TEOS 97%, Fluka) and HCl (37% in water, Aldrich) was used as reaction catalyst, triethylamine (Merck) and acetic acid (Merck) were used to synthesise PIL.

2.2 Preparation of PIL

Triethylamine acetate was obtained according to the literature.[31] A typical polymerization procedure is described as follows. Acetic acid (30.025 g) was added dropwise into triethylamine (50.595 g) at 353 K. After stirring for 5 h, PIL which was yellow was obtained. PIL was characterized by ^{1}H NMR.^{1}H-NMR ($CDCl_3$) δ：7.979 (s, 1H, -NH), 2.762 (s, 3H, CH_3COO-), 1.277-1.86 (t, 2H, -CH_2-), 0.86 (s, 3H, -CH_3), which is consistent with literature reports.

2.3 Synthesis of micro/mesoporous materials

In a typical synthesis, 4 g P123 and an appropriate amount of PIL were completely dissolved in water; its pH was controlled by HCl (2 M). Under strong stirring, 9 g tetraethyl orthosilicate (TEOS) was dripped slowly. After stirring at 313 K for 24 h, the whole slurry was transferred into an autoclave for aging at an appropriate temperature for 48 h. The PIL and organic components were extracted by ethanol and then water in an oven overnight. The white as-synthesized solid powders were then calcined at 823 K for 6 h in ambient air, with a heating rate of 3 K·min^{-1}.

Similarly, a series of micro/mesoporous materials were synthesized by changing the ratio of PILs and temperature during synthesis. The final products were denoted as PIL-X-Y, in which X represents the mass ratio of PIL to (P123+PIL); Y represents

the aging temperature, respectively. As a comparison, samples either without P123 (denoted as PIL) or using water to replace PIL (denoted as P123) were also prepared.

2.4 Catalysts preparation

1 g of micro/mesoporous materials were added into the mixture of 20 mL ethyl alcohol and 0.4 g of 12-Tungstophosphoric acid at 333 K. The mixture continuously stirred until ethyl alcohol steamed. The obtained white solid was dried at 393 K overnight and calcined in air at 573 K for 4 h.

2.5 Catalytic tests

The alkylation reactions were carried out in a continuously stirred oil batch reactor under 393 K. Styrene (6 g), *o-xylene* (45 g) (quality ratio of *o-xylene* to styrene, 7.5:1) and 1.02 g of catalyst were introduced in a three-neck 100 mL round-bottom flask equipped with a condenser for 3 h. Firstly, the mixture of the small amount of *o-xylene* and the desired amount of catalyst were added to the round-bottom flask at 393 K, the mixture of a certain amount of styrene and the remaining *o-xylene* then dropwise into the flask for 2 h. The final reaction mixture remained for another 1 h. After the reaction, unreacted *o-xylene* was distilled out under atmospheric pressure, and then the obtained liquid was denoted by crude product which was analyzed with GC-9890A gas chromatograph equipped with OV-1 capillary column and a flame ionization detector (FID). The yield of PXE was defined as follows:

$$\text{yield of PXE}(\%) = \frac{\text{actual product weight}}{\text{theoretical product weight}} \times 100\%$$

actual product weight = crude product weight × PXE (chromatography) %

2.6 Characterization

The structure of the calcined samples was characterized by an X-ray powder diffractometor (Rigaku, RINT-Ultima III) using Cu Kα radiation with 40 kV and 200 mA. All scans were continuous and run between 2θ values of 0-5°. The N_2 physical adsorption and desorption isotherms were adopted at 77 K to obtain surface areas with ASAP 2020 apparatus (Micromertics USA) by means of the Brunauer-Emmett-Teller (BET) method. The pore size distribution in mesopore range was analyzed by the BJH (Barrett-Joyner-Halenda) method using the Halsey equation for multilayer thickness. Micropore volume was calculated by the t-plot method. Transmission Electron Microscopy (TEM) was performed on FEI Tecnai G20 instrument. Infrared spectra were recorded on a Bruker Tensor 27 (German) using DRIFT techniques, scanned from 4000 to 400 cm^{-1}. The sample was ground with KBr and pressed into a thin wafer. The samples were evacuated at 573 K for 4 h before the measurement. Scanning electron microscopy (SEM) images were recorded on a JEOL JSM-5600L SEM Instrument with a working distance of 3-4 mm and an electron voltage of 3.0 kV. The size distributions of micelles were determined by dynamic laser light scattering (DLS) on a Malvern Nano-ZS, with a detecting angle of 90°.

3. Results and discussion

3.1 Effect of the PIL content

Fig. 1 around here

The XRD patterns of the samples induced by PIL/P123 co-templates are shown in figure 1. When the mass ratio of PIL to (P123+PIL) is 30% and 40% (PIL-30, PIL-40), three well-resolved diffraction peaks which include a strong reflection at 2θ=0.86° for

d_{100} and two other weaker reflections at 2θ=1.55° and 2θ=1.71° respectively for d_{110} and d_{200} are observed in the curve, which is a typical pattern characterizing the hexagonal arrangement of SBA-15. Only one broad diffraction peak with a much lower intensity is preserved for PIL-50, indicating its less ordered structure. No other obvious diffraction peak is observed with increasing the content of PIL, stating a poor periodicity for PIL-60 and PIL-70.

Fig. 2 around here

N_2 adsorption isotherms of the calcined samples in Fig. 2A exhibit the typical IV adsorption. The presence of a pronounced hysteresis loop in the isothermals indicates the intersection network of porous structures. At very low relative pressure p/p^0, an increase at the adsorption isothermal of all materials proves the presence of micropores. With the increase of PIL content, the pressure onset of the hysteresis gradually shifts to lower values from 0.6 (PIL-40) to 0.4 (PIL-70), which illustrates pore size shrinkage. Distortion of the characteristic hysteresis loop of PIL-70 demonstrates the loss of ordered pore structure, which agrees with the XRD result. There is a clear hysteresis loop in the isothermals of PIL, indicating protic ionic liquid can self-assemble to micelles which act as the mesoporous templates at higher PIL concentration.

Fig. 2B shows the pore size distribution calculated by BJH model based on desorption curves. Two peaks are observed from the pore size distributions of the sample PIL-60, whereas the others have only one peak. The difference may be caused by the existence of PIL micro scale micelles and P123 mesoscale micelles. From the data above, it can

be concluded that PIL and P123 are miscible and can form mixed micelles at lower PIL concentration, while, PIL micelles can separated from the mixed micelles with the increase of PIL concentration. And two different scale micelles which induce the micro/mesoporous material is formed. And The sample PIL-70 only has one peak at 3.8 nm, indicating the structure of ordered channel has been destroyed. That certifies the function of ionic liquid for the material structure.

Table 1 around here

The characteristic data on the samples are summarized in Table 1. From Table 1, it can be seen that with increasing PIL, the average pore size of each sample is 7.14, 5.14, 4.35, 3.32 nm, respectively. Among them, PIL-40 and PIL-30 possess extremely large pore volume of 1.23, 1.31 $cm^3 \cdot g^{-1}$, which are larger than that of the pure SBA-15 of 1.10 $cm^3 \cdot g^{-1}$. This phenomenon indicates the positive contributions of PIL to the volume.

Fig. 3 around here

The TEM images of the calcined sample prepared at 393 K show the structure of the samples obtained with different PIL content, meaning P123/PIL templates can induce micro/mesoporous composites. The images for PIL-30 and PIL-40 show very ordered mesoporous structure, these mesopores are arranged in a hexagonally ordered array. The order-degree of samples decreases with increasing the content of PIL. If making a local enlargement, the wall filled with the cycle-like micropores is found. The image 3C of the sample PIL-50 lacks orderliness because of the existence of PIL, which is consistent with the XRD result. And the hexagonally ordered array structure of

PIL-70 totally disappear, only disordered worm-like mesopores can be found in the image 3E, illustrating the excess of PIL affect the conformation of samples. The morphology of the PIL-40 particles prepared at 373 K is shown in the SEM image 3F, which exhibits worm-like shapes.

Fig. 4 around here

Fig. 4 shows the size distribution of P123/PIL micelles in aqueous solutions with different PIL concentration at room temperature. Only one peak could be found in the sample P123 and PIL-40 at 18 and 20 nm, respectively. While, the average diameter of PIL-40 has a higher value than that of P123, demonstrating the PIL maybe around the P123 micelles owing to the hydrogen bonding. Another new peak at 7 nm appears with increasing the PIL concentration, representing the PIL may self-assembly form a new micelles, which is consistent with pore size distribution of PIL-60.

3.2 Effect of the hydrothermal temperature

Fig. 5 around here

The low-angle XRD patterns of the samples induced by PIL/P123 co-templates at different temperature are shown in Fig. 5. When the temperature is 393 K and 373 K, three well-resolved diffraction peaks are observed in the curve, which corresponding to the (100), (110) and (200) reflections. While, the intensity of PIL-40-373 is much lower than PIL-40-393. It means that the ordered mesoporous structure is affected by temperature. Three peaks are disappeared when the temperature is 353 K, which shows a poor periodicity of the sample's structure.

Fig. 6 around here

Table 2 around here

The N_2 adsorption isotherms of the calcined samples at different temperature are shown in Fig. 6A. Pronounced hysteresis loop characterizing the cylindrical mesopores can be observed at 393 K or 373 K, representing that the samples have a ordered porous structure. While, the adsorption of PIL-40-393 is higher than that of PIL-40-373. The distortion of hysteresis loop indicates the loss of the ordered pore structure at 353 K, which according to the XRD results. Fig. 6B shows the pore size distribution calculated by BJH model based on desorption curves. The mesopore size distribution of PIL-40-373 is similar with that of PIL-40-393 whose mesopore size is about 6.3 nm. While, from the Table 2, it is can be seen that PIL-40-373 has a t-plot micropore area of 404 $m^2 \cdot g^{-1}$, which is larger than other samples. When the temperature increase to 393 K, there is still a t-plot micropore area of 21 $m^2 \cdot g^{-1}$, certifying the effect of PIL microporous template. Through the analysis, it is known that the ordered mesoporous channels with small amounts of micropores can be obtained at 393 K, and materials which not only possess more micropores but also remain the hexagonally ordered array structure are induced at a low temperature of 373 K. When the temperature decreases to 353 K, the material with disordered structure is obtained. Thus, the hydrothermal temperature is a significant factor to obtain the micro/mesoporous material.

Fig. 7 around here

Fig. 7 shows the TEM images of PIL-40 synthesised at different temperature. A little disordered structure can be seen when the temperature is 353 K. The two-dimensional

hexagonal structure has been destroyed. When the temperature increases to 373 K or 393 K, the mesopores are arranged in an ordered array as observed in images 7B and 7C. And both of the samples show uniformly distributed pores with the pore size estimated to be 6.3 nm from the image, which is consistent with the result of N_2 gas sorption. A part of the walls of mesoporous channels are destroyed a little in the enlarged insert, which may duing to the existence of worm-like micropores. Compared with PIL-40-393, PIL-40-373 has a higher t-plot micropore area of 404 $m^2 \cdot g^{-1}$. Thus, the favorable temperature to synthesis the micro/mesoporous SBA-15 materials is 373 K.

Formation mechanism of hierarchical micro/mesoporous silica: In aqueous systems, mesopores were produced in an analogous liquid templating approach. Micropores and mesopores were obtained with the elimination of PIL and P123, respectively. P123 micelles have a hydrophobic core and a hydrophilic head group. There is a strong interaction between PIL and P123 mainly due to the hydrogen bond. And the inorganic network also has a strong interaction with the polar domain of the PIL molecules, thus creating micropores. The ammonium-based ionic liquid (triethylamine acetate) can act as multiple roles of cosolvent, cosurfactant as well as salt in the system. When the content of PIL is low, the co-solvent and co-surfactant functions are dominant. PIL and P123 are miscible and can form mixed micelles in aqueous solution. The short chains of PIL probably incline to swell the P123 micelles. Thus, the average diameter of P123/PIL mixed aggregates may shift to a higher value. Which is analogous to the function of the diameter expander, reagent

1,3,5-trimethylbenzene (TMB). In the case of P123/TMB mixed micelles, TMB molecules are totally solubilized in the core of P123 micelles, which obviously forms the swollen P123 micelles, consequently the size of mixed micelles can be higher than P123 micelles. Protic Ionic liquids can separated from the mixed micelles at higher concentration of protic ionic liquid. And the large micelles induced by numbers of ionic liquid micro scale micelles act as the mesoporous template. This phenomenon is certified by pore size distribution of PIL-60 which has two peaks (3.9 nm, 7.7 nm). And the structure of the final sample is influenced by PIL as well. The mesoporous structure becomes disordered with increasing the content of protic ionic liquid, which is confirmed by the XRD pattens and TEM results. PIL micelles are dominant in the solution under the high PIL concentration, and the P123 micelles almost disappear, which is confirmed by the size distribution curve of PIL-70. The presence of disordered micropores may contribute to the disappearance of the (110) and (200) peaks in the XRD patterns of the final samples. The formation mechanism of the micro/mesoporous silica material which is based on the interaction between PIL and P123 is schematically presented in Fig. 8.

Fig. 8 around here

3.3 Catalytic activity of micro/mesoporous materials supported HPW

Fig. 9 around here

The IR spectra of the pure HPW, PIL-X and HPW/PIL-X-Y are shown in Fig. 9A.

IR peaks of pure HPW show approximately at 1080 (P-O in the central tetrahedron), 980 (terminal W=O) and 890 and 800 (W-O-W) cm^{-1} corresponding to asymmetric

vibration associated with Keggin ion. IR peak of SBA-15 at 3440 cm^{-1} is stretching frequency for hydroxyl and silicon hydroxyl), 1630 cm^{-1} peak is bending vibration peak for O-H of adsorbed water, 1080 cm^{-1}, 808 cm^{-1} and 461 cm^{-1} peaks are vibration absorption peaks for Si-O-Si, including 1080 cm^{-1} peak is the strong asymmetric stretching vibration absorption peak of Si-O-Si, 968 cm^{-1} peak is bending vibration peak for silicon hydroxyl. Fig. 9B presents the IR spectra of all different HPW/PIL-X-Y samples. It can be seen that the IR bands at approximately 980 cm^{-1}, 890 cm^{-1} and 800 cm^{-1} are clearly observed. This indicates the primary structure of 12-Tungstophosphoric acid is preserved even after immobilization at the surface of PIL-X-Y.

Table 3. around here

The catalytic performance of different carriers with HPW were investigated owing to the carriers contain high surface area and narrow size distribution which are favorable conditions for the reaction. Sheng *et al.*[32] found that pure HPW showed high catalytic performance for the reaction, while, it was difficult for recovery. HPW/SBA-15 showed the low product yield (68.3%) in their work. From Table 3, it is found that the support itself has no catalyst performance and other samples exhibit the much higher catalytic properties than those of HPW/SBA-15 in their work. Among the catalysts investigated, HPW/PIL-30-393 with large pore size of the support exhibited the best catalytic performance. Thus, the catalytic activity may change along with the pore size of supports because large pore size material is conducive to the macromolecular reaction. So, suitable pore size may contribution to the high catalytic performance.

Fig. 10 around here

Stability and reusability of the catalyst are significant for any catalytic system. The reusability of the HPW/PIL-30-393 and HPW/SBA-15 catalysts has been evaluated by carrying out the reaction with used catalyst under the optimized conditions. After each run, the catalyst was recovered by filtration, then washed with ethanol, dried and calcined at 573 K for 4 h, and used again. The data obtained are summarized in Fig. 10. It can be seen only 15% reduction in the activity is observed after 4 runs on the HPW/PIL-30-393 catalyst. In contrast, the deactivation of HPW/SBA-15 catalyst is much faster and PXE yield drops to 40% after the fourth reaction cycle. The poor catalytic stability of HPW/SBA-15 may be due to the possibility that HPW leaching from the catalyst support into the liquid reaction system may result in the low conversion. Furthermore, micropores of HPW/PIL-30-393 may be another reason for better stability.

4. Conclusion

In summary, a series of micro/mesoporous silica materials are obtained using P123 and PIL (triethylamine acetate) as co-templates. The structure of the final materials was investigated by two important factors: the PIL content and hydrothermal temperature. The formation mechanism of the micro/mesoporous silica which is based on the interaction between PIL and P123 is tentatively elucidated. At low concentration of PIL, PIL and P123 can form mixed micelles in aqueous solution because of the hydrogen bond. PIL may separate from P123 micelles and form mesoscale micelles with the increase of PIL content. The results showed that the

sample PIL-40-373 not only possessed a t-plot micropore area of 404 $m^2 \cdot g^{-1}$ but also remained the hexagonally ordered array structure. A serious of micro/mesoporous materials supported HPW catalysts were obtained, and their catalytic performances were investigated in the alkylation of *o-xylene* with styrene. Alkylation results showed that catalysts had much higher product yield and longer catalytic life, which might be due to the large pore size of the support and the strong interaction between the HPW and the supports.

Acknowledgments

The authors are grateful to the financial supports of National Natural Science Foundation of China (Grant No.21306023, 21376051, 21106017 and 51077013), Fund Project for Transformation of Scientific and Technological Achievements of Jiangsu Province of China (Grant No. BA2011086), Key Program for the Scientific Research Guiding Found of Basic Scientific Research Operation Expenditure of Southeast University (Grant No. 3207043101) and Instrumental Analysis Fund of Southeast University.

References

1. D. Zhao, J. Feng, Q. Huo, N. Melosh, G. H. Frederickson, B. F. Chmelka, G. D. Stucky, *Science*, 1998, **279**, 548-552.
2. Z. L. Hua, J. Zhou, J. L. Shi, *Chem Commun*, 2011, **47**, 10536-10547.
3. J. G. Li, R. B. Lin, S. W. Kuo, *RSC Adv*, 2013, **3**, 17411-17423.
4. Y. Ooi, S. Bhatia, *Micropor Mesopor Mater*, 2007, **102**, 310-317.
5. T. Welton, *Chem Rev*, 1999, **99**, 2071-2083.
6. D. Zhang, A. Duan, Z. Zhao, C. Xu, *J Catal*, 2010, **274**, 273-286.
7. H. C. Xin, J. Zhao, S. T. Xu, J. P. Li, W. P. Zhang, X. W. Guo, E. J. M. Hensen, Q. H. Yang, C. Li, *J Phys Chem C*, 2010, **114**, 6553.
8. L. M. Xiong, J. L. Shi, L. X. Zhang, M. Y. Nogami, *J Am Chem Soc*, 2007, **129**, 11878-11879.
9. X. Chen, Z. Q. Sun, L. L. Zheng, Z. M. Chen, Y. F. Wang, N. Fu, K. Zhang, X. Yan, H. Liu, L. Jiang, B. Yang, *Adv Mater*, 2004, **16**, 1632-1636.
10. K. Egeblad, C. H. Christensen, M. Kustova, C. H. Christensen, *Chem Mater*, 2008, **20**,

946-960.
11. R. Sheldon, *Chem Commun*, 2001, 2399-2407.
12. H. Li, P. S. Bhadury, B. Song, S. Yang, *RSC Adv*, 2012, **2**, 12525-12551.
13. C. C. Ke, J. Li, X. J. Li, Z. G. Shao, B. L. Yi, *RSC Adv*, 2012, **2**, 8953-8956.
14. C. M. Gordon, *Appl Catal a-Gen*, 2001, **222**, 101-117.
15. P. Wasserscheid, W. Keim, *Angew Chem Int Edit*, 2000, **39**, 3772-3789.
16. K. Binnemans, *Chem Rev*, 2005, **105**, 4148-4204.
17. C. K. Lee, H. W. Huang, I. J. B. Lin, *Chem Commun*, 2000, 1911-1912.
18. T. L. Merrigan, E. D. Bates, S. C. Dorman, J. H. Davis, *Chem Commun*, 2000, 2051-2052.
19. Y. Zhou, M. Antonietti, *Adv Mater*, 2003, **15**, 1452-1455.
20. Y. Zhou, J. H. Schattka, M. Antonietti, *Nano Lett*, 2004, **4**, 477-481.
21. J. Hu, J. X. Yin, T. S. Lin, G. T. Li, *J Chem Educ*, 2012, **89**, 284-285.
22. F. Gao, J. Hu, C. J. Peng, H. L. Liu, Y. Hu, *Langmuir*, 2012, **28**, 2950-2959.
23. J. Hu, F. Gao, Y. Z. Shang, C. J. Peng, H. L. Liu, Y. Hu, *Micropor Mesopor Mater*, 2011, **142**, 268-275.
24. T. L. Greaves, A. Weerawardena, C. Fong, C. J. Drummond, *Langmuir*, 2007, **23**, 402-404.
25. A. Kumar, P. Venkatesu, *RSC Adv*, 2013, **3**, 362-367.
26. T. L. Greaves, A. Weerawardena, C. Fong, I. Krodkiewska, C. J. Drummond, *J Phys Chem B*, 2006, **110**, 22479-22487.
27. Z. F. Chen, T. L. Greaves, R. A. Caruso, C. J. Drummond, *J Mater Chem*, 2012, **22**, 10069-10076.
28. X. L. Sheng, Y. M. Zhou, Y. W. Zhang, Y. Z. Duan, M. W. Xue, *Catal Lett*, 2012, **142**, 360-367.
29. X. L. Sheng, Y. M. Zhou, Y. W. Zhang, M. W. Xue, Y. Z. Duan, *Chem Eng J*, 2012, **179**, 295-301.
30. X. L. Sheng, Y. M. Zhou, Y. L. Yang, Y. W. Zhang, Z. W. Zhang, S. J. Zhou, X. Q. Fu, S. Zhao, *RSC Adv*, 2014, **4**, 30697-30703.
31. J. Y. Weng, C. M. Wang, H. R. Li, Y. Wang, *Green Chem*, 2006, **8**, 96-99.
32. X. L. Sheng, J. Kong, Y. M. Zhou, Y. W. Zhang, Z. W. Zhang, S. J. Zhou, *Micropor Mesopor Mater*, 2014, **187**, 7-13.

Figure/Table Captions

Fig. 1: XRD patterns of the samples induced by PIL/P123 co-templates at 393 K.

Fig. 2: (A) N_2 adsorption-desorption isotherms, (B) pore size distributions calculated by BJH model based on desorption curves of the calcined samples induced by P123/PIL co-templates at 393 K.

Fig. 3: The images of the calcined samples induced by P123/PIL at 393 K. The TEM image of (A) PIL-30, (B) PIL-40, (C) PIL-50, (D) PIL-60, (E) PIL-70, (F) the SEM image of PIL-40. The insets are the local enlargements with the same enlargement scale.

Fig. 4: Size distribution of P123/PIL aqueous solutions determined by DLS.

Fig. 5: XRD patterns of the PIL-40 at different temperature.

Fig. 6: (A) N_2 adsorption-desorption isotherms, (B) pore size distributions calculated by BJH model based on desorption curves of the calcined samples induced by PIL-40 co-templates at different temperature.

Fig. 7: TEM images of the PIL-40 at different temperature. (A) 353 K, (B) 373 K, (C) 393 K. The insets are the local enlargements with the same enlargement scale.

Fig. 8: The template mechanism of IL cationic $[N(CH_2CH_3)_3]^+$ and P123 (A) synergism for mesoporous material at lower PIL content, and (B) for the micro/mesoporous materials at higher PIL content.

Fig. 9: (A) FT-IR spectra of pure HPW, PIL-X and HPW/PIL-X and (B) FT-IR spectra of different HPW/PIL-X-Y samples.

Fig. 10: Catalytic Stability of the HPW/PIL-30-393 and HPW/SBA-15 catalysts in the alkylation of *o-xylene* with styrene (Reaction conditions: *o-xylene*: styrene = 7.5:1, reaction temperature = 393 K, reaction time = 3.0 h, catalyst loading = 20% (w/w of styrene).

Table 1: Physicochemical properties of the calcined samples induced by P123/PIL co-templates at 393 K.

Table 2: Physicochemical properties of the calcined samples.

Table 3: Activity of various supported HPW catalysts[a] in alkylation of *o-xylene* with styrene.

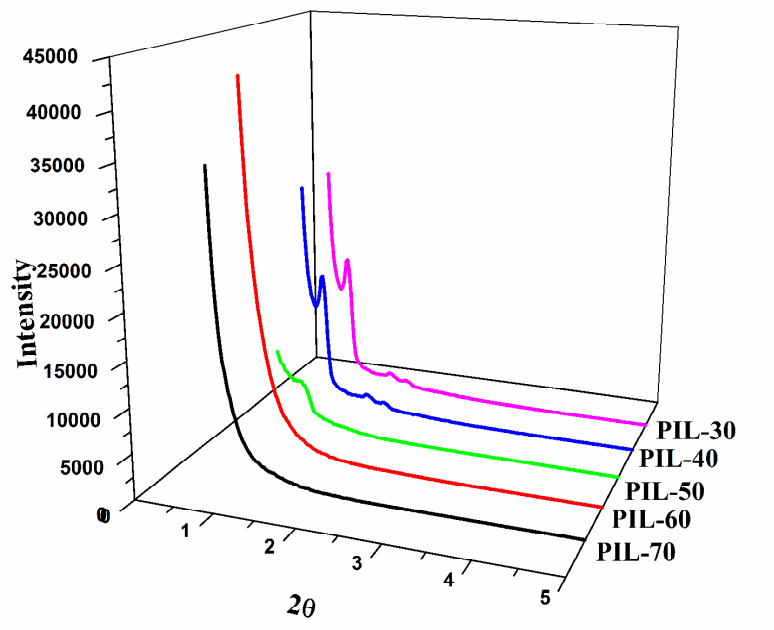

Fig. 1. XRD patterns of the samples induced by PIL/P123 co-templates at 393 K.

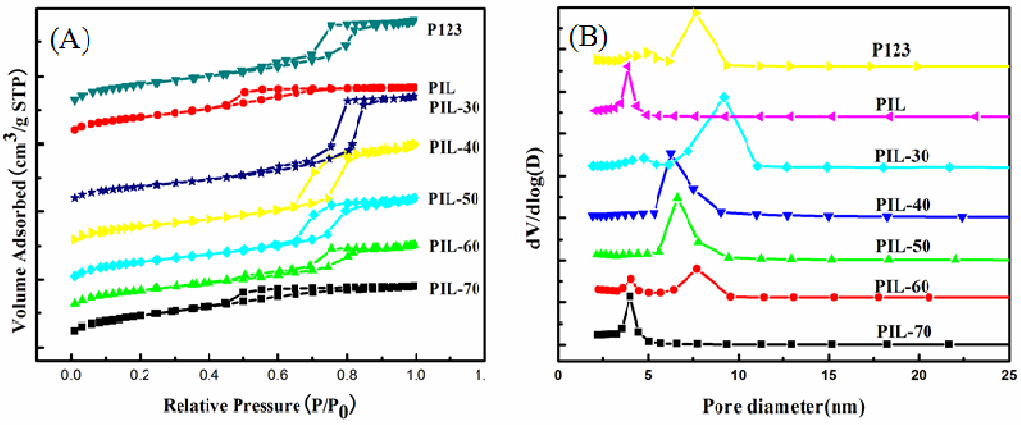

Fig. 2. (A) N_2 adsorption-desorption isotherms, (B) pore size distributions calculated by BJH model based on desorption curves of the calcined samples induced by P123/IL co-templates at 393 K.

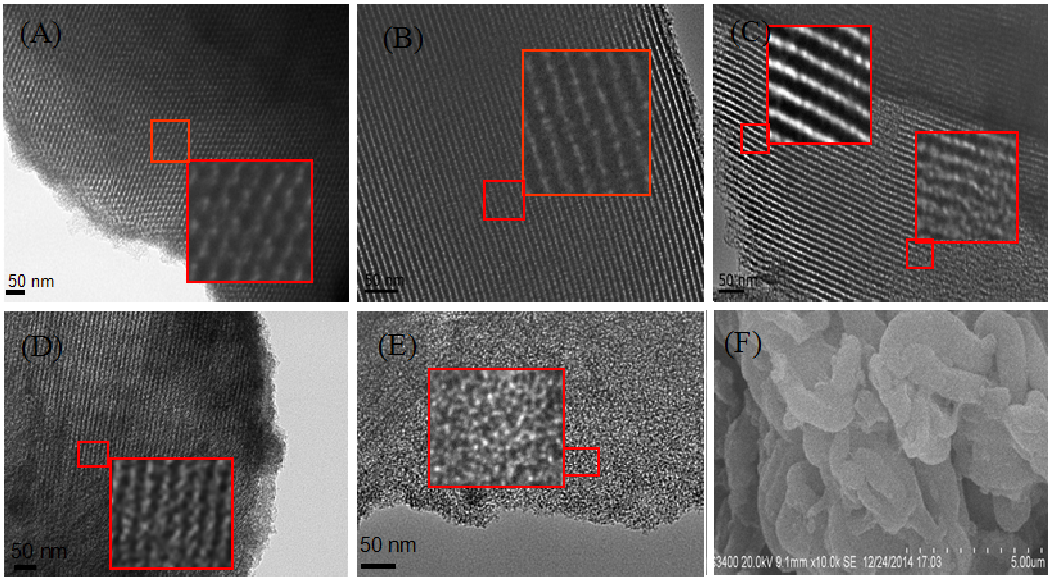

Fig. 3. The images of the calcined samples induced by P123/PIL at 393 K. The TEM image of (A) PIL-30, (B) PIL-40, (C) PIL-50, (D) PIL-60, (E) PIL-70, (F) the SEM image of PIL-40. The insets are the local enlargements with the same enlargement scale.

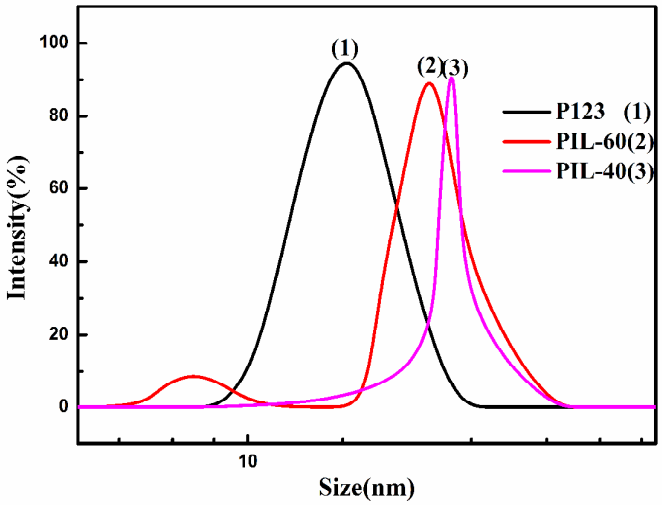

Fig. 4. Size distribution of P123/PIL aqueous solutions determined by DLS.

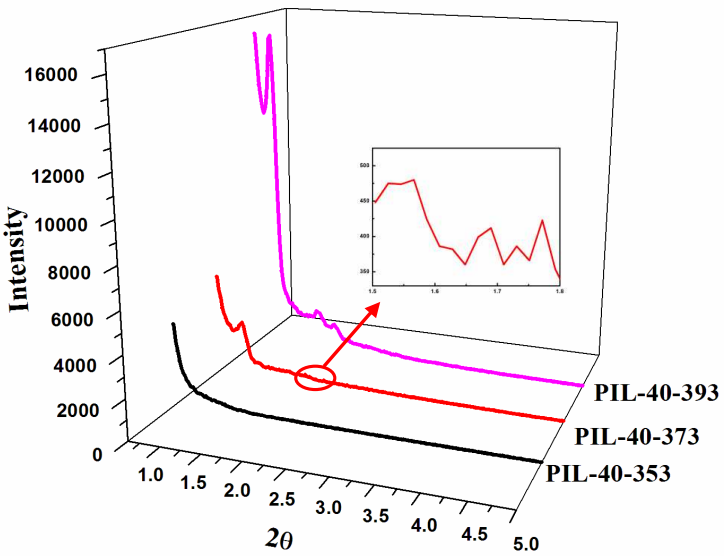

Fig. 5. XRD patterns of the PIL-40 at different temperature.

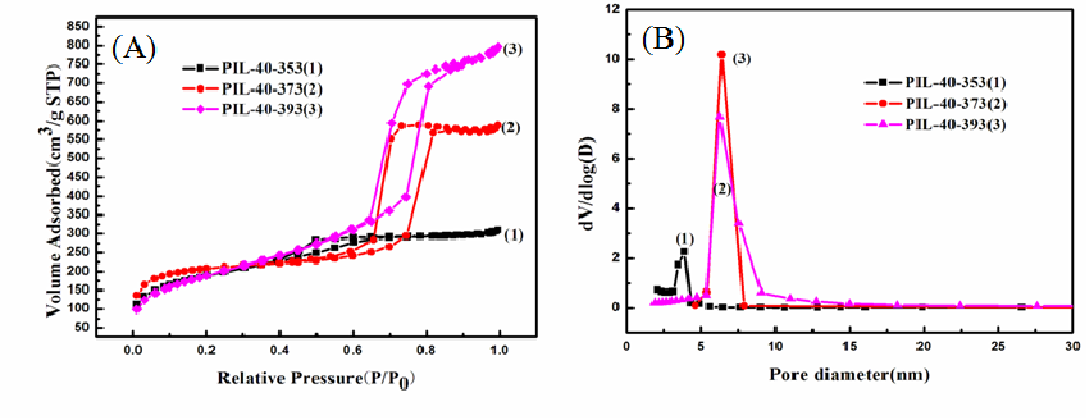

Fig. 6. (A) N_2 adsorption-desorption isotherms, (B) pore size distributions calculated by BJH model based on desorption curves of the calcined samples induced by PIL-40 co-templates at different temperature.

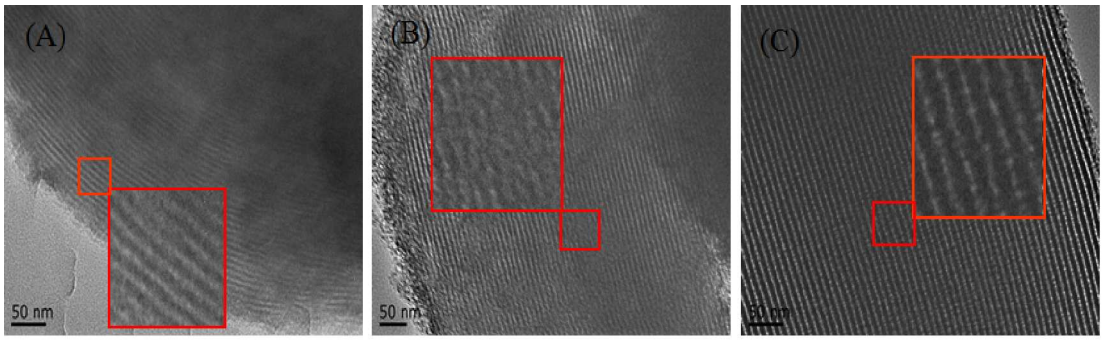

Fig. 7. TEM images of the PIL-40 at different temperature. (A) 353 K, (B) 373 K, (C) 393 K. The insets are the local enlargements with the same enlargement scale.

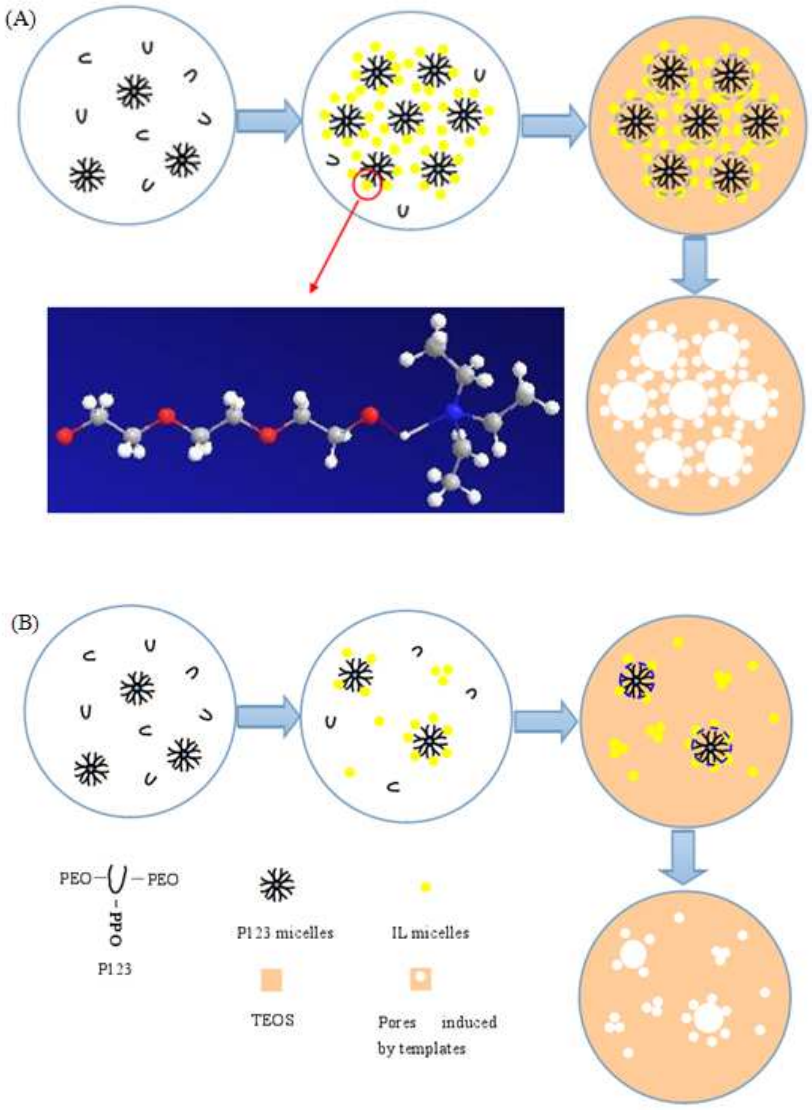

Fig. 8. The template mechanism of IL cationic $[N(CH_2CH_3)_3]^+$ and P123 (A) synergism for mesoporous material at lower PIL content, and (B) for the micro/mesoporous materials at higher PIL content.

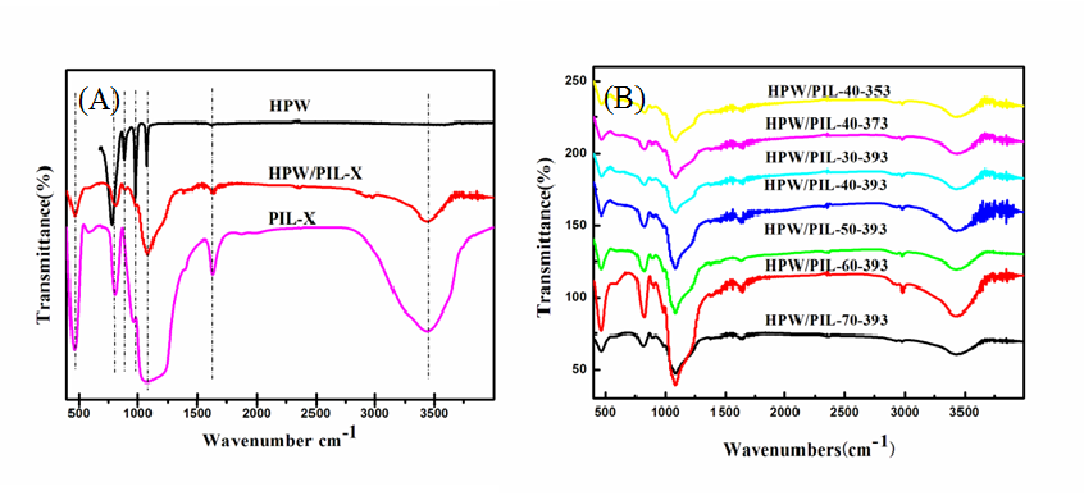

Fig. 9. (A) FT-IR spectra of pure HPW, PIL-X and HPW/PIL-X and (B) FT-IR spectra of different HPW/PIL-X-Y samples.

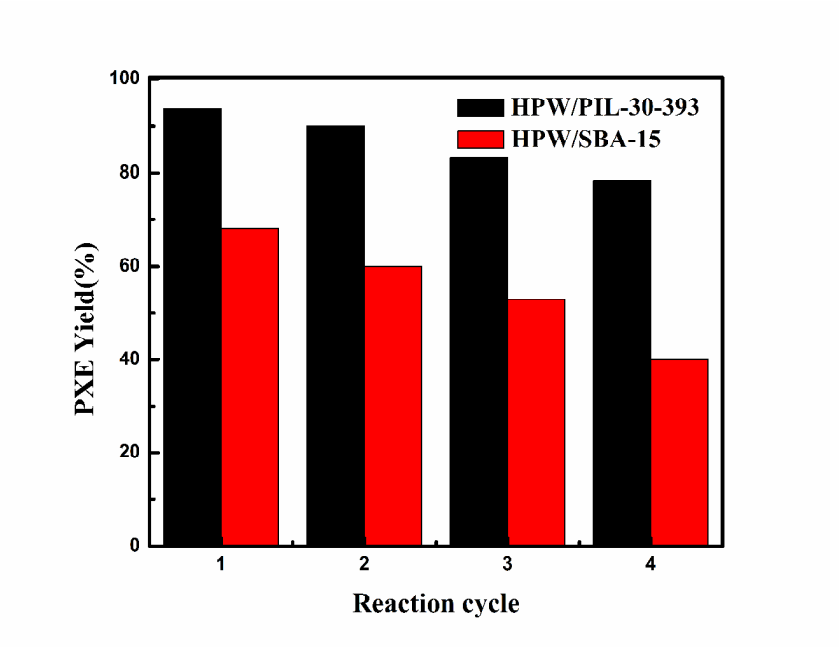

Fig. 10. Catalytic Stability of the HPW/PIL-30-393 and HPW/SBA-15 catalysts in the alkylation of *o-xylene* with styrene (Reaction conditions: *o-xylene*: styrene = 7.5:1, reaction temperature = 393 K, reaction time = 3.0 h, catalyst loading = 20% (w/w of styrene)

Table 1. Physicochemical properties of the calcined samples induced by P123/PIL co-templates at 393 K

Sample name	BET Surface Area (m^2/g)	Pore Volume (cm^3/g)	Average Pore Size(nm)
PIL-70	838	0.70	3.32
PIL-60	796	0.86	4.35
PIL-50	844	1.08	5.14
PIL-40	691	1.23	7.14
PIL-30	681	1.32	7.73
PIL	720	0.65	3.59
P123	881	1.10	5.01

Table 2. Physicochemical properties of the calcined samples induced by PIL-40 co-templates at different temperature

Sample name	Temperature (K)	BET Surface Area (m^2/g)	Micropore Surface Area (m^2/g)	Pore Volume (cm^3/g)	Average Pore Size(nm)
PIL-40-353	353	676	133	0.48	2.84
PIL-40-373	373	722	404	0.91	5.05
PIL-40-393	393	691	21	1.23	7.14

Table 3. Activity of various supported HPW catalysts[a] in alkylation of *o-xylene* with styrene.

Catalyst	Yield[b](%)	Selectivity[c](%)
PIL-40	–	–
HPW/PIL-70-393	85.46	85.66
HPW/PIL-60-393	86.28	86.47
HPW/PIL-50-393	89.42	89.57
HPW/PIL-40-393	90.29	90.55
HPW/PIL-30-393	93.80	94.57
HPW/PIL-40-373	86.52	86.72
HPW/PIL-40-353	80.38	80.56

[a] Reaction conditions: *o-xylene* : styrene = 7.5:1, reaction temperature = 393 K, reaction time = 3.0 h, catalyst loading = 20% (w/w of styrene).

[b] Isolated yield based on the amount of styrene.

[c] Target product: all products.